Radiation Dosimetry and Biodistribution in Monkey and Man of ^{11}C-PBR28: A PET Radioligand to Image Inflammation

Amira K. Brown[1], Masahiro Fujita[1], Yota Fujimura[1], Jeih-San Liow[1], Michael Stabin[2], Yong H. Ryu[1,3], Masao Imaizumi[1], Jinsoo Hong[1], Victor W. Pike[1], and Robert B. Innis[1]

[1]Molecular Imaging Branch, National Institute of Mental Health, Bethesda, Maryland; [2]Department of Radiology and Radiological Sciences, Vanderbilt University Medical Center Nashville, Nashville, Tennessee; and [3]Department of Nuclear Medicine, Yonsei University Medical College, Seoul, South Korea

^{11}C-PBR28 ([*methyl*-^{11}C]*N*-acetyl-*N*-(2-methoxybenzyl)-2-phenoxy-5-pyridinamine) is a recently developed radioligand to image peripheral benzodiazepine receptors (PBRs) in brain. The aim of this study was to estimate the human radiation doses of ^{11}C-PBR28 based on biodistribution data in monkeys and humans. In addition, we scanned 1 human subject who fortuitously behaved as if he lacked the PBR binding protein. **Methods:** Whole-body PBR images were acquired after intravenous bolus administration of ^{11}C-PBR28 in 7 healthy humans (651 ± 111 MBq) and 2 rhesus monkeys (370 ± 59.9 MBq). One monkey was scanned after receptor blockade with PK 11195 (10.7 mg/kg intravenously). **Results:** For typical subjects (subjects 1–6), the 3 organs with highest exposure were those with the high PBR densities (kidneys, spleen, and lungs), and the effective dose was 6.6 μSv/MBq. The unusual subject (subject 7) had 60%–90% less uptake in these 3 organs, resulting in 28% lower effective dose. The activity in the baseline monkey scans was greater than that in humans for organs with high PBR densities. For this reason, the human effective dose was overestimated by 60% with monkey biodistribution data. The monkey with receptor blockade had an overall distribution qualitatively similar to that of the unusual human subject (subject 7), with decreased exposure to lungs, kidney, and spleen. **Conclusion:** The effective dose of ^{11}C-PBR28 was modest and was similar to that of several other ^{11}C-radioligands. Lack of receptor binding in the unusual human subject and in the monkey with receptor blockade decreased exposure to organs with high PBR densities and enhanced uptake in excretory and metabolic pathways.

Key Words: translocator protein (18 kDa); source organ; ^{11}C-PBR28; PET

J Nucl Med 2007; 48:2072–2079
DOI: 10.2967/jnumed.107.044842

The peripheral benzodiazepine receptor (PBR) is a mitochondrial protein that is highly expressed in phagocytic inflammatory cells: macrophages in the periphery and activated microglia in the central nervous system (*1*). Imaging of PBRs can localize inflammation in brain associated with increased densities of these phagocytic cells. For example, several PET studies using the PBR radioligand ^{11}C-PK 11195 have localized inflammation associated with acute neurologic and neurodegenerative disorders (*2*). In addition to their high expression in phagocytic cells, PBRs are located on the mitochondrial outer membrane in several organs, including kidney, lung, and heart wall (*3*). PBRs in these peripheral organs will temporarily bind PBR ligands and reduce the amount that is delivered to brain.

A new class of high-affinity PBR ligands has been synthesized with an aryloxyanalide backbone (*4*) (*5–8*), instead of the isoquinoline structure of PK 11195. Our laboratory synthesized one such aryloxyanalide, ^{11}C-PBR28 ([*methyl*-^{11}C]*N*-acetyl-*N*-(2-methoxybenzyl)-2-phenoxy-5-pyridinamine), which gave promising imaging results in monkeys and rats. After injection of ^{11}C-PBR28 in monkeys, uptake of radioactivity in brain could be quantified relative to plasma concentrations and had a high percentage of specific receptor binding (>85% of total brain radioactivity) (*9*). Furthermore, PET with ^{11}C-PBR28 in rats could localize and quantify inflammation surrounding a stroke induced with occlusion of a cerebral artery (*10*).

The primary goals of the current study were to estimate the human radiation-absorbed dose from ^{11}C-PBR28 and to determine whether results from monkeys accurately predict those obtained directly from humans. In addition, we scanned one unusual human subject who appeared to lack binding of ^{11}C-PBR28 to PBR in brain. Decreased uptake in brain was not caused by rapid metabolism, as the plasma clearance of ^{11}C-PBR28 in arterial samples was similar to that of other healthy subjects. We later performed whole-body imaging on this subject and found minimal uptake in peripheral organs with high densities of PBRs—namely, lung, kidney, spleen, and heart wall. In summary, this subject behaved as if he lacked the PBR binding protein or as if his PBRs had minimal affinity for ^{11}C-PBR28. We do

Received Jul. 2, 2007; revision accepted Sep. 7, 2007.
For correspondence or reprints contact: Amira K. Brown, PhD, Molecular Imaging Branch, National Institute of Mental Health, 31 Center Dr., Room B2/B34, Bethesda, MD 20892-2035.
E-mail: amirabrown@mail.nih.gov

not know the reason(s) for the unusual finding in this healthy individual. Nevertheless, this subject provided the opportunity to assess the effect of receptor availability on radiation exposure.

MATERIALS AND METHODS

Radiopharmaceutical Preparation

^{11}C-PBR28 was prepared by the ^{11}C-methylation of its desmethyl analog with ^{11}C-iodomethane, itself prepared from cyclotron-produced ^{11}C-carbon dioxide, and purified with reverse-phase high-performance liquid chromatography (HPLC). Preparations were conducted according to our exploratory Investigational New Drug Application 73,935, submitted to the U.S. Food and Drug Administration and a copy of which is available at: http://kidb.bioc.cwru.edu/snidd/. The radioligand was obtained in high radiochemical purity (>99%), and the specific activity at the time of injection = 183 ± 76.2 GBq/μmol (n = 9 batches), as assessed by analytic reverse-phase HPLC with these and subsequent numeric data expressed as mean ± SD.

Human Subjects

Our use of ^{11}C-PBR28 in human subjects was approved the Radiation Safety Committee of the National Institutes of Health and the Institutional Review Board of the National Institute of Mental Health. Seven healthy volunteers participated: 4 males and 3 females, 31 ± 9 y of age, 77 ± 15 kg body weight. All subjects were free of current medical and psychiatric illness on the basis of history, physical examination, electrocardiogram (ECG), urinalysis including drug screening, and blood tests (complete blood count, serum chemistries, thyroid function test, and antibody screening for syphilis, HIV, and hepatitis B). Approximately 24 h after the PET scan, subjects returned to repeat the urinalysis and blood tests.

Subject 7 showed no binding to ^{11}C-PBR28. He was a 26-y-old Latin American male in excellent health, with no significant prior medical history and taking no medications at the time of the whole-body scan.

Animal Subjects

Two male rhesus monkeys (4.5 and 5.0 kg) were scanned. To allow intubation, animals were anesthetized with propofol (1.2–4 mg/kg intravenously), ketamine (10–15 mg/kg intramuscularly), and glycopyrrolate (0.15–0.2 mg/kg intravenously). After transportation to the PET suite, the animals were anesthetized with isoflurane (1.5%–2%) for the duration of the scanning experiment. To minimize the effects of ketamine, scans started at least 90 min after its administration. Body temperature was controlled by an air-circulating heating device (Bair Hugger, model 505; Arizant Healthcare). The ECG, pulse, and respiration rate were monitored throughout the experiment.

Human PET and Image Analysis

Subjects underwent transmission and dynamic emission scans on an Advance tomograph (GE Healthcare). Transmission scans using ^{68}Ge rods were obtained on 7 segments of 15 cm each, the axial view of the scanner, from the top of the head to the midthigh. Each transmission scan lasted 3 min. To minimize extraneous motion, all subjects wore a mask that affixed their head in a single position and had their arms and abdomen wrapped with body-restraining sheets. Blood pressure, pulse, and respiration rates were obtained before the administration of ^{11}C-PBR28 and at 4 points during the emission scans.

After intravenous bolus administration of ^{11}C-PBR28 (651 ± 111 MBq), dynamic emission scans of 14 frames were acquired by serial imaging of the body in the 7 contiguous segments. The durations of the initial frames were 15 s at each segment, followed by frames of increasing duration, with six 3-s intervals to move the bed to the next section and 13 s to return back to the first bed position. The total scanning time was ~120 min (4 × 15 s, 3 × 30 s, 3 × 60 s, 3 × 2 min, and 1 × 4 min for each of the 7 body segments).

The 245 (35 slices × 7 beds) original tomographic PET images of human subjects were reinterpolated into isotropic voxels and compressed into whole-body images in 2 different ways, 2-dimensional (2D) planar and bisected: (a) 2D planar. All voxels were compressed into a single image in the coronal orientation; as shown in Figure 1. (b) Bisected: Voxels were roughly divided through the midcoronal plane and compressed into an anterior and a posterior planar image in the coronal orientation.

Image analysis was performed using PMOD 2.8 (pixelwise modeling computer software; PMOD Group). Regions of interest were drawn in source organs that could be identified on 6 of the subjects: brain, heart, lungs, spleen, liver, kidneys, gallbladder (visible in only 3 subjects), and urinary bladder. To avoid the contamination of high lung activity into the heart, we compressed 17–20 transverse slices from the tip of the apex to the base of the myocardium in head to feet direction. One unusual subject (subject 7) had visible organ activity in only the liver, gallbladder, and

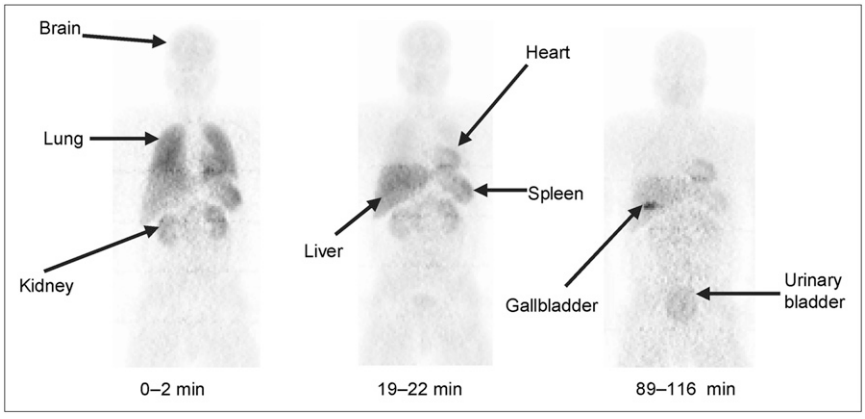

FIGURE 1. Compressed anteroposterior whole-body 2D planar images of subject 4, a typical healthy individual. Images were obtained at 0–2, 19–22, and 89–116 min after intravenous injection of 703 MBq ^{11}C-PBR28.

urinary bladder. Large regions of interest were placed to ensure that all accumulated radioactivity in each organ was included.

Animal PET and Image Analysis

Three whole-body baseline scans were acquired on the GE Advance tomograph in 4 segments of the body (head to thigh) in frames of increasing duration (75 s to 15 min) (4×15 s, 4×30 s, 8×1 min, 4×2 min, 2×4 min) for a total scan time of ~120 min. A urinary catheter was inserted and clamped so that the radioactivity overlaying the bladder represented the total urinary excretion during the scanning interval. Data acquisition during PET started immediately after the intravenous injection of ^{11}C-PBR28 (370 ± 59.9 MBq) via the posterior tibal vein.

A preblocking scan was performed on 1 monkey after its baseline scan, in which nonradioactive PK 11195 (10.7 mg/kg intravenously) was injected 3 min before the radioligand. The pretreatment interval of 3 min was selected because the uptake and washout of PK 11195 is rapid in monkey brain (*11*).

The tomographic PET images were compressed into a single 2D planar image as previously described. Regions of interest were drawn on visually identifiable source organs: brain, heart, lungs, spleen, kidneys, liver, and urinary bladder.

Residence Time Calculations for Humans and Monkeys

The organ activity values were corrected for recovery relative to a large region of interest over the entire body for each frame. The injected activity value for each source organ at every time point was multiplied by 100/X, where X is the measured recovery for the individual frame. In humans, the measured recovery averaged 93% for all frames. In monkeys, the measured recovery was only 33% for the first frame but was an average of 90% for the remaining frames. The low recovery of the first frame was presumably due to the injection site being below the field of view.

The "remainder of body" was calculated for each time point as the decayed value of the original injected activity minus that in the identified source organs.

Time–activity curves for the source organs were plotted as the percentage of injected activity versus time. For simplicity, we chose to use a trapezoidal integration to calculate the area under the curve up to the termination of acquisition for each source organ, including the urinary bladder. The area under the curve after the acquisition of the last image to infinity was calculated by assuming that the decline in radioactivity after this time point occurred by physical decay only, without any further biologic clearance. The area under the curve of the percentage injected activity from time zero to infinity is equivalent to the residence time for the human.

The residence times for all of the source organs were summed and subtracted from the fixed theoretic value of $t_{1/2}/\ln 2 = 0.49$ h to calculate the residence time of the remainder in the body for each subject. $t_{1/2}$ is the radioactive half-life of ^{11}C (0.33 h).

Note that residence time is calculated from the area under the plot of decayed activity versus time. In contrast, Figures 3, 4, and 6 in this article plot decay-corrected activities to show uptake and washout of radioactive compounds.

For monkeys, residence times were calculated as described but converted into corresponding human values by multiplication with a factor to scale organ and body weights: $(b_m/o_m) \times (o_h/b_h)$, where b_m and b_h are the body weights of monkey and human, respectively; and o_m and o_h are the organ weights of monkey and human, respectively. Organ weights were obtained from a textbook for the rhesus monkey (*12*) and from *Taber's Cyclopedic Medical Dictionary* for humans (*13*).

Organ Absorbed Dose

Radiation-absorbed doses were calculated by entering the residence times of all source organs for each subject and monkey into the OLINDA 1.0/EXM computer program (*14*) using the model for a 70-kg adult male. We were unable to fit the accumulated urinary bladder activity to a biexponential curve and, thus, did not use the dynamic bladder model. Instead, residence times of the bladder were calculated in the same fashion as the other source organs.

RESULTS

Human Subjects with Expected Biodistribution

Intravenous injection of ^{11}C-PBR28 (carrier PBR28, 0.019 ± 0.006 μg/kg, $n = 5$) produced no clinically observable effects. Blood pressure, pulse, and respiratory rate during the 2 h after injection as well as blood and urine tests on the next day had clinically insignificant changes. After injection of ^{11}C-PBR28, brain, lungs, liver, heart, kidneys, spleen, and urinary bladder were visually identified as source organs with moderate-to-high activity in most subjects (Fig. 1). The gallbladder was not visualized in 3 subjects, and the spleen, lungs, and kidneys were not visualized in 1 subject—namely, unusual subject 7 (Fig. 2).

Lungs had the highest uptake, with a peak value of 35% injected activity ($n = 6$) during the first frame acquisition (0–2 min). Peak values of the percentage injected activity in liver, kidneys, brain, spleen, heart, and gallbladder were 15%, 14%, 5%, 4.5%, 3.7%, and 1%, respectively, all occurring within 10 min (Figs. 3A and 3B; excluding heart). Subject 7 had significantly less uptake in organs with high densities of PBR—namely, lung, heart, brain, spleen, and kidneys (Figs. 3C and 3D). For subject 7, the peak lung uptake (10%) was lower than the average lung uptake of subjects 1–6 (35%), and the washout from his brain was faster than that in the other volunteers (Fig. 4).

The residence times of organs listed in (Table 1) were calculated from 2D planar images in healthy subjects 1–6 and separately for the unusual subject 7. Cumulative activity in the urinary bladder could not be fitted with a mono- or biexponential curve. Thus, a dynamic bladder model was not applied. For subjects 1–6, the effective dose was 6.6 μSv/MBq, and the 3 organs with highest radiation-absorbed doses were kidneys (53 μSv/MBq), spleen (26 μSv/MBq), and lungs (22 μSv/MBq) (Table 2). The use of 2D planar images may have significantly increased the activity of some organs by including tissue anterior and posterior to the organ. Of the identified sources, kidneys and heart were probably the most contaminated by adjacent activity and their residence times were also calculated from images with less compression. Because of its location, the kidney was recalculated with the posterior of the 2 bisected images. The heart was also recalculated with the superior–inferior compression of the chest. See the Materials and Methods for details on the image analysis. Compared with 2D planar analysis, these 2 methods

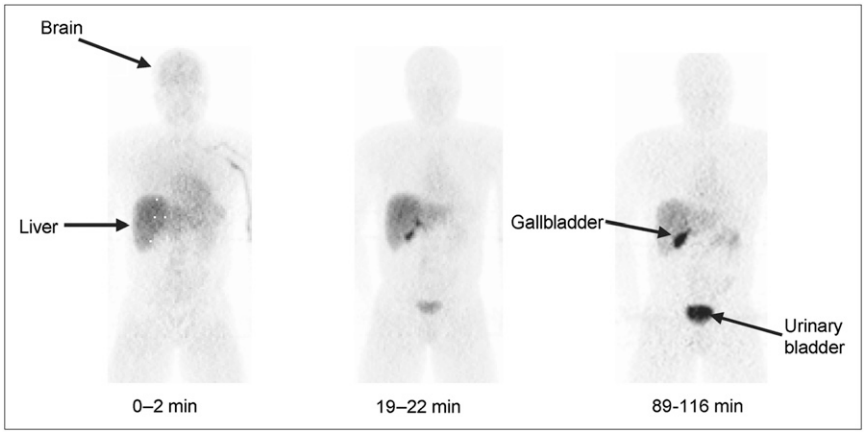

FIGURE 2. Compressed anteroposterior whole-body 2D planar images for unusual healthy subject 7 with minimal or no ^{11}C-PBR28 binding. Images were obtained approximately 0–2, 19–22, and 89–116 min after intravenous injection of 544 MBq.

with less contamination decreased the residence times and radiation exposures of kidney and heart. For example, the radiation exposure of heart decreased from 11.2 to 7.8 μSv/MBq and that of kidney decreased from 52.6 to 29.9 μSv/MBq. Nevertheless, the effective dose remained 6.6 μSv/MBq. In a similar manner, the dose to the kidneys decreased 43%, from 52.6 to 29.9 μSv/MBq. Nevertheless, the effective dose was minimally affected, changing from 6.6 to 6.2 μSv/MBq.

Human Subject with Unexpected Biodistribution

Compared with subjects 1–6, subject 7 had decreased activity in organs with high PBR densities—that is, brain, lungs, heart, spleen, and kidneys (Figs. 3C and 3D). In fact, spleen, lungs, and kidneys could not be identified visually in this subject (Fig. 2). Furthermore, the activities in liver and gallbladder of subject 7 were much higher than the mean of subjects 1–6 (Figs. 3C and 3D).

The dosimetry estimates in subject 7 reflected biodistribution and tended to decrease radiation burden to organs with high PBR densities and increased radiation burden to organs associated with excretion and metabolism. For example, among organs with high PBR densities, the doses were decreased in brain (31%), lungs (56%), heart (29%), spleen (91%), and kidneys (94%) relative to that of subjects 1–6. In contrast, doses were increased to liver (65%), gallbladder wall (218%), and urinary bladder wall (20%). Overall, the effective dose was 28% less compared with that of subjects 1–6 (supplemental Table 1; supplemental Tables 1 and 2 are available online only at http://jnm.snmjournals.org).

Monkey Biodistribution

Injection of ^{11}C-PBR28 caused no change in ECG, heart, or respiration rates. Gallbladder, lungs, spleen, heart, brain, kidneys, liver, and urinary bladder were visually identified as organs with moderate-to-high activity (Fig. 5). Uptake of

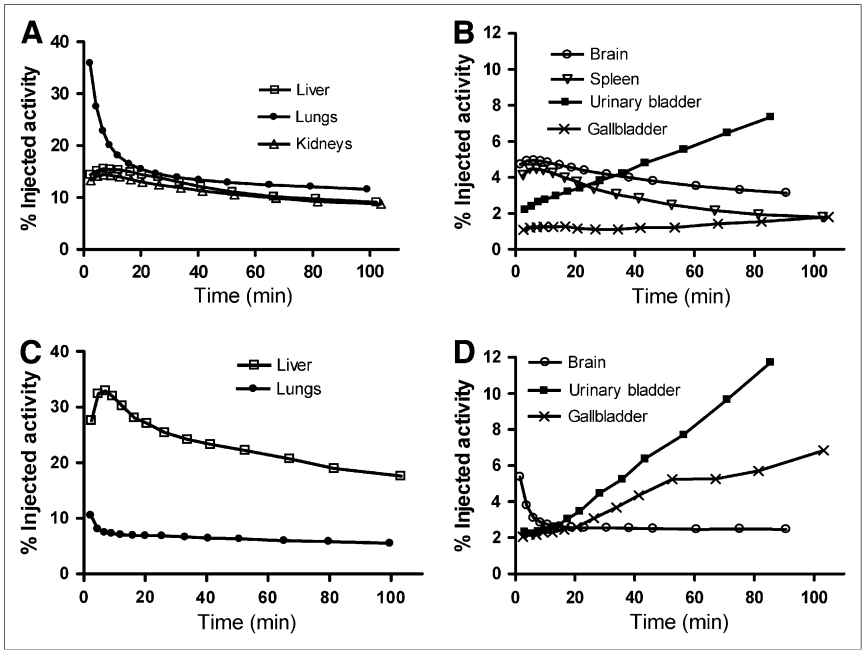

FIGURE 3. Decay-corrected time–activity curves for visually identifiable organs from the average of subjects 1–6 (A and B) and the unusual subject 7 (C and D). Kidneys (C) and spleen (D) could not be seen in subject 7. Graph becomes too cluttered if SD error bars are included. Distribution of data is exemplified by the % coefficient of variation (SD/mean) at 60 min for A and B, with lungs at 40%, liver at 28%, gallbladder at 29%, and brain at 35%.

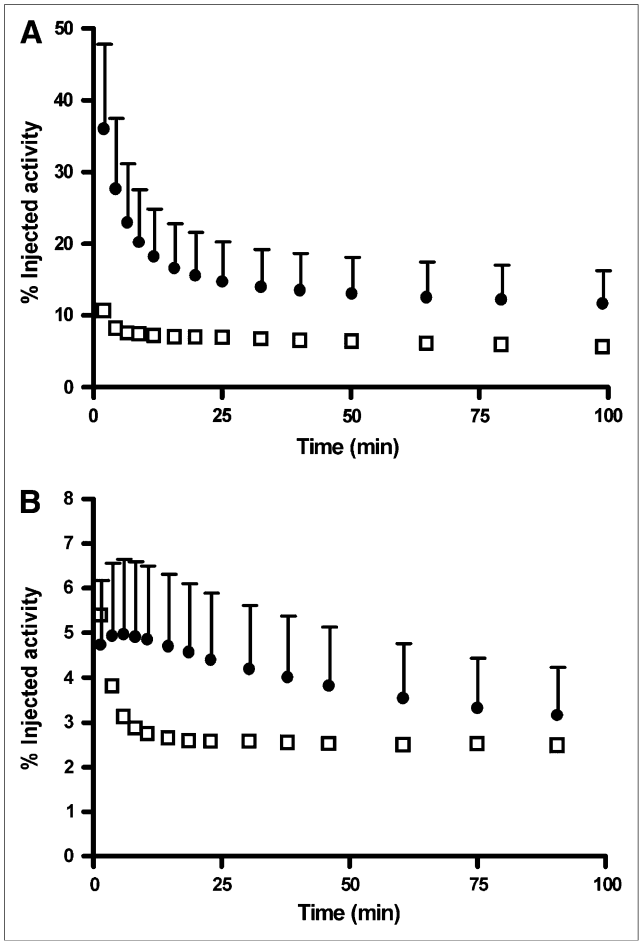

FIGURE 4. Decay-corrected time–activity curves of lung (A) and brain (B) in subjects 1–6 (●) and unusual subject 7 (□). Symbols represent mean + SD for subjects 1–6.

^{11}C-PBR28 was highest in the lungs, with a peak of 50% injected activity occurring during the first frame (0–1.15 min). Peak uptake in kidneys, heart, liver, brain, and urinary bladder were 19.5%, 7%, 10%, 4.2%, and 0.8% standardized uptake value, respectively (Fig. 6).

TABLE 1
Residence Times of Source Organs

Organ	Residence time (h)		
	Subjects 1–6	Subject 7	Ratio*
Brain	0.020 ± 0.007	0.013	0.7
Heart wall	0.011 ± 0.004	0.017	1.5
Kidneys	0.058 ± 0.023	—	—
Liver	0.069 ± 0.015	0.122	1.8
Gallbladder	0.004 ± 0.003	0.015	4.0
Urinary bladder	0.018 ± 0.011	0.021	1.2
Lungs	0.083 ± 0.031	0.033	0.4
Spleen	0.016 ± 0.004	—	—
Remainder in body	0.213 ± 0.074	0.270	1.3

*Ratio of subject 7 to mean of subjects 1–6.
Values are mean ± SD of 6 subjects. Subject 7 lacked PBR binding and was analyzed separately.

TABLE 2
Radiation Dosimetry Estimates for ^{11}C-PBR28 in 6 Healthy Subjects

Organ	Dose	
	μSv/MBq	mrem/mCi
Adrenals	4.1 ± 0.2	15.0 ± 0.9
Brain	4.8 ± 1.5	17.9 ± 5.5
Breasts	1.9 ± 0.2	7.1 ± 0.7
Gallbladder wall	12.2 ± 6.8	45.3 ± 25
Lower large intestine wall	1.9 ± 0.3	7.0 ± 1.2
Small intestine	2.3 ± 0.3	8.4 ± 1.2
Stomach	2.7 ± 0.2	10.0 ± 0.7
Upper large intestine wall	2.4 ± 0.3	8.7 ± 1.2
Heart wall	11.2 ± 3.0	41.6 ± 11
Kidneys	52.6 ± 20	194.7 ± 75
Liver	13.1 ± 2.6	48.4 ± 9.5
Lungs	22.0 ± 7.6	81.6 ± 28
Muscle	1.9 ± 0.2	7.1 ± 0.9
Ovaries	2.0 ± 0.2	7.4 ± 1.3
Pancreas	3.9 ± 0.1	14.6 ± 0.5
Red marrow	2.1 ± 0.1	7.6 ± 0.5
Osteogenic cells	2.5 ± 0.5	9.2 ± 1.8
Skin	1.4 ± 0.3	5.2 ± 1.0
Spleen	25.9 ± 5.6	95.9 ± 21
Testes	1.5 ± 0.3	5.4 ± 1.3
Thymus	2.3 ± 0.2	8.5 ± 0.9
Thyroid	1.7 ± 0.4	6.1 ± 1.3
Urinary bladder wall*	13.3 ± 6.7	49.2 ± 25
Uterus	2.3 ± 0.2	8.5 ± 0.7
Total body	2.9 ± 0.1	10.7 ± 0.4
Effective dose equivalent	11.0 ± 2.4	40.7 ± 8.9
Effective dose	6.6 ± 1.7	24.3 ± 6.3

*Dynamic urinary bladder model was not used.
Values are expressed as mean ± SD.

Human residence times were extrapolated from 3 imaging sessions in 2 monkeys (Table 3). Similar to the human bladder, cumulative urinary activity in the monkey could not be fitted with a biexponential curve; thus, the dynamic bladder model was not applied. The human effective dose estimated from monkey whole-body imaging was 10.3 μSv/MBq (supplemental Table 1). The 3 organs with the highest radiation burden (μSv/MBq) were lungs (70.5), kidneys (43.1), and brain (19.5).

Comparison of Monkey and Human Biodistribution Data

The overall distribution of activity was similar in the baseline monkey and typical healthy humans (subjects 1–6). For example, both had high uptake in lungs, kidney, and spleen (Figs. 1 and 5A). To estimate human dosimetry from the monkey biodistribution data, organ weight and body mass were used for allometric scaling (Materials and Methods). The human effective dose was overestimated by 60% using the monkey data, with exposures to individual organs both over- and underestimated. The overestimation of effective dose was primarily caused by higher exposures in 3 organs, all of which have high PBR densities. Compared with

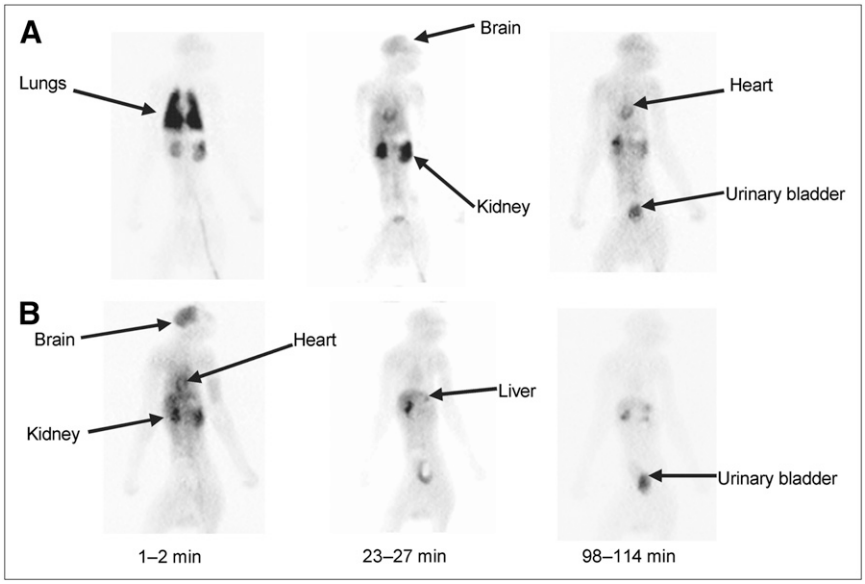

FIGURE 5. Compressed anteroposterior whole-body 2D planar images in same monkey at baseline (A) and after receptor blockade (B). For the latter, nonradioactive PK 11195 (10.7 mg/kg intravenously) was administered 3 min before the radioligand. Injected activity of ^{11}C-PBR28 was 348 MBq (A) and 332 MBq (B).

human biodistribution results, the monkey dose was elevated in brain (4-fold), lung (3.2-fold), and heart (1.8-fold, rightmost column, supplemental Table 1).

DISCUSSION

To our knowledge, this article reports the first-in-human use of ^{11}C-PBR28, a potential cellular marker of inflammation. On the basis of human biodistribution data, ^{11}C-PBR28 caused only modest radiation exposure, with an effective dose of 6.6 μSv/MBq.

Effect of Receptor Availability

We examined the effect of receptor availability in both monkeys using preblockade and in humans via a single unusual subject. The blockade or absence of these receptor reservoirs had similar effects in both species—that is, decreased radiation to organs with high densities of PBRs and increased radiation to organs associated with metabolism and excretion. For example, radiation dose decreased 60%–70% to lung and 70%–90% to spleen (supplemental Table 1), and both of these organs have high densities of PBRs. In the absence of receptor binding, the plasma concentration of the radioligand increases and more radiopharmaceutical is exposed to organs of elimination. Thus, radiation burden to liver was increased 70%–90% in human and monkey, respectively (supplemental Table 1). Receptor blockade also increased urinary elimination of radioactivity, with radiation to urinary bladder increased 70% in monkey and 20% in

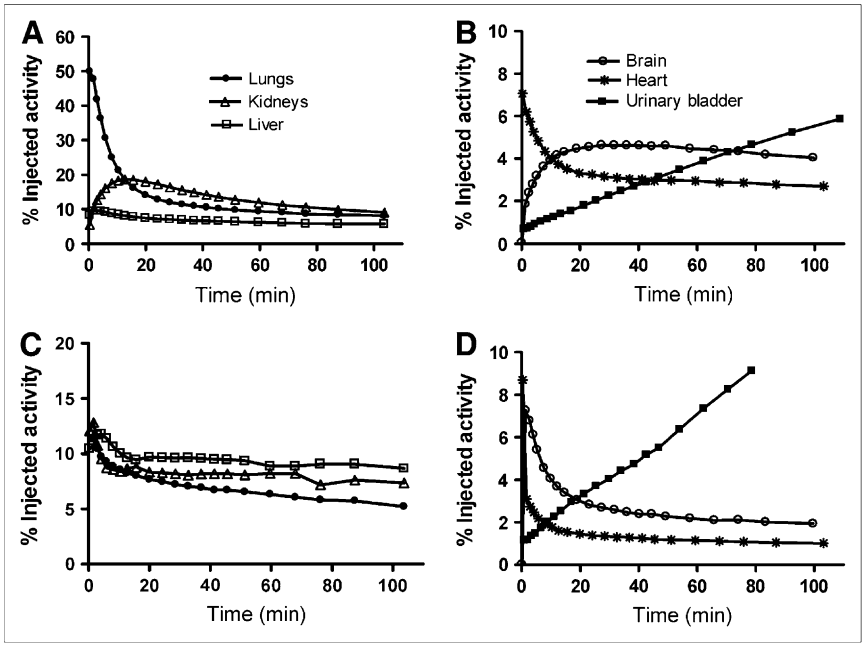

FIGURE 6. Decay-corrected time–activity curves for visually identifiable organs in monkeys from the average of 3 baseline (A and B) and 1 receptor-blocked study (C and D).

TABLE 3
Monkey Residence Times of Identified Source Organs

Organ	Residence time (h)	
	Baseline	Preblocked
Brain	0.086 ± 0.006	0.024
Heart wall	0.021 ± 0.003	0.008
Kidneys	0.048 ± 0.008	0.042
Urinary bladder	0.012 ± 0.003	0.018
Lungs	0.277 ± 0.01	0.067
Liver*	0.020	0.051
Spleen	0.006 ± 0.004	—
Remainder in body	0.022 ± 0.12	0.282

*Liver was visible in only 1 study.

Residence times in baseline conditions were averaged over 3 studies using 2 monkeys. One preblocked study was performed by injecting 10.7 mg/kg of nonradioactive PK 11195 three minutes before the radioligand.

human. In summary, both monkey and human showed expected effects of receptor availability. The radioligand's distribution, which by definition is the temporary sequestration of a drug, was decreased to organs with high receptor densities, and its elimination was increased via metabolism and excretion.

Monkey as Model for Human

Is the monkey an adequate model for human dosimetry? Our biodistribution studies in baseline monkeys (i.e., without receptor blockade) overestimated the effective dose in humans by 60% (supplemental Table 1, far right column). Although a sizeable overestimation, the resulting effective dose (10.3 μSv/MBq) was still within the overall dose range of 12 representative ^{11}C-labeled radioligands for brain imaging (supplemental Table 2). The higher effective dose to monkeys compared with humans was caused primarily by greater exposure to brain (4-fold), lung (3.2-fold), and heart wall (1.8-fold) (supplemental Table 1, far right column). These organs all have high PBR densities (*15–18*). In summary, the 60% overestimation of human effective dose was likely caused by the higher PBR binding potential in monkey brain, lung, and heart wall.

Comparison with Other Radioligands

Calculated as the effective dose from human biodistribution studies, the radiation exposure from ^{11}C-PBR28 (6.6 μSv/MBq) was similar to that of 11 other radioligands used in brain imaging (supplemental Table 2). Of the 12 ligands listed, 11 are tightly distributed, with a range of 4.3 to 7.0 μSv/MBq. ^{11}C-WAY100635, a radioligand for serotonin 5-HT$_{1A}$ receptors, is a marked outlier, with an effective dose of 14.1 μSv/MBq (supplemental Table 2). The high effective dose of ^{11}C-WAY 100635 was caused by the rapid and substantial urinary excretion of radioactivity. About 80% of injected activity accumulated in the bladder within 1 h and caused unusually high doses to this organ and kidneys. In fact, the rapidity of the urinary excretion of ^{11}C-WAY 100635 may provide a practical upper limit on radiation exposures for ^{11}C agents excreted via this route. In the absence of a single predominant mode of elimination (e.g., urinary excretion for ^{11}C-WAY 100635), ^{11}C-labeled radioligands are likely to have an effective dose of about 6–7 μSv/MBq.

CONCLUSION

The novel radioligand ^{11}C-PBR28 caused relatively modest radiation burdens, similar to several other ^{11}C-radioligands used for brain imaging. For unknown reasons, one healthy subject had negligible uptake in organs with high PBR densities. The uptake in this unusual human subject was similar to that in a monkey with preblockade of receptors using high doses of nonradioactive PK 11195. Blockade or absence of receptors was associated with decreased radiation burden to organs with high PBR densities and enhanced uptake in excretory and metabolic pathways.

ACKNOWLEDGMENTS

This research was supported in part by the Intramural Program of NIMH (project Z01-MH-002852-01). We gratefully acknowledge Robert Gladding, CNMT, for PET imaging of monkeys; the staff of the PET department for successful completion of this study; Janet Sangare, MS, C-RNP, Alicja Lerner, MD, PhD, and Amanda Farris, BA, for human subject recruitment; and PMOD Technologies (Adliswil, Switzerland) for providing its image analysis and modeling software.

REFERENCES

1. Papadopoulos V, Baraldi M, Guilarte TR, et al. Translocator protein (18 kDa): new nomenclature for the peripheral-type benzodiazepine receptor based on its structure and molecular function. *Trends Pharmacol Sci.* 2006;27:402–409.
2. Venneti S, Lopresti BJ, Wiley CA. The peripheral benzodiazepine receptor (translocator protein 18 kDa) in microglia: from pathology to imaging. *Prog Neurobiol.* 2006;80:308–322.
3. Gavish M, Bachman I, Shoukrun R, et al. Enigma of the peripheral benzodiazepine receptor. *Pharmacol Rev.* 1999;51:629–650.
4. Okuyama S, Chaki S, Yoshikawa R, et al. Neuropharmacological profile of peripheral benzodiazepine receptor agonists, DAA1097 and DAA1106. *Life Sci.* 1999;64:1455–1464.
5. Fujimura Y, Ikoma Y, Yasuno F, et al. Quantitative analyses of ^{18}F-FEDAA1106 binding to peripheral benzodiazepine receptors in living human brain. *J Nucl Med.* 2006;47:43–50.
6. Ikoma Y, Yasuno F, Ito H, et al. Quantitative analysis for estimating binding potential of the peripheral benzodiazepine receptor with ^{11}C-DAA1106. *J Cereb Blood Flow Metab.* 2007;27:173–184.
7. Maeda J, Suhara T, Zhang MR, et al. Novel peripheral benzodiazepine receptor ligand ^{11}C-DAA1106 for PET: an imaging tool for glial cells in the brain. *Synapse.* 2004;52:283–291.
8. Zhang MR, Maeda J, Furutsuka K, et al. ^{18}F-FMDAA1106 and ^{18}F-FEDAA1106: two positron-emitter labeled ligands for peripheral benzodiazepine receptor (PBR). *Bioorg Med Chem Lett.* 2003;13:201–204.
9. Imaizumi M, Briard E, Zoghbi SS, et al. Kinetic evaluation in nonhuman primates of two new PET ligands for peripheral benzodiazepine receptors in brain. *Synapse.* 2007;61:595–605.
10. Imaizumi M, Kim HJ, Zoghbi SS, et al. PET imaging with ^{11}C-PBR28 can localize and quantify upregulated peripheral benzodiazepine receptors associated with cerebral ischemia in rat. *Neurosci Lett.* 2007;411:200–205.
11. Venneti S, Lopresti BJ, Wang G, et al. PET imaging of brain macrophages using the peripheral benzodiazepine receptor in a macaque model of neuroAIDS. *J Clin Invest.* 2004;113:981–989.

12. Bourne GH. *The Rhesus Monkey.* New York, NY: Academic Press; 1975.
13. Venes D, Taber CW. *Taber's Cyclopedic Medical Dictionary.* 20th ed. Philadelphia, PA: F.A. Davis Co.; 2005.
14. Stabin MG, Sparks RB, Crowe E. OLINDA/EXM: the second-generation personal computer software for internal dose assessment in nuclear medicine. *J Nucl Med.* 2005;46:1023–1027.
15. Anholt RR, Pedersen PL, De Souza EB, Snyder SH. The peripheral-type benzodiazepine receptor: localization to the mitochondrial outer membrane. *J Biol Chem.* 1986;261:576–583.
16. Basile AS, Skolnick P. Tissue specific regulation of "peripheral-type" benzodiazepine receptor density after chemical sympathectomy. *Life Sci.* 1988;42: 273–283.
17. Chelli B, Falleni A, Salvetti F, Gremigni V, Lucacchini A, Martini C. Peripheral-type benzodiazepine receptor ligands: mitochondrial permeability transition induction in rat cardiac tissue. *Biochem Pharmacol.* 2001;61:695–705.
18. Cox DA, Ellinor PT, Kirley TL, Matlib MA. Identification of a 17-kDa protein associated with the peripheral-type benzodiazepine receptor in vascular and other smooth muscle types. *J Pharmacol Exp Ther.* 1991;258:702–709.

JNM The Journal of NUCLEAR MEDICINE

Radiation Dosimetry and Biodistribution in Monkey and Man of ^{11}C-PBR28: A PET Radioligand to Image Inflammation

Amira K. Brown, Masahiro Fujita, Yota Fujimura, Jeih-San Liow, Michael Stabin, Yong H. Ryu, Masao Imaizumi, Jinsoo Hong, Victor W. Pike and Robert B. Innis

J Nucl Med. 2007;48:2072-2079.
Published online: November 15, 2007.
Doi: 10.2967/jnumed.107.044842

The Journal of Nuclear Medicine is published monthly.
SNMMI | Society of Nuclear Medicine and Molecular Imaging
1850 Samuel Morse Drive, Reston, VA 20190.
(Print ISSN: 0161-5505, Online ISSN: 2159-662X)

SNMMI SOCIETY OF NUCLEAR MEDICINE AND MOLECULAR IMAGING